Extraction of Front- and Rear-Interface Recombination in Silicon Double-Heterojunction Solar Cells by Reverse Bias Transients

Alexander H. Berg, *Student Member, IEEE*, Ken A. Nagamatsu, *Member, IEEE*, and James C. Sturm, *Fellow, IEEE*

***Abstract*— We present a method, based upon reverse-recovery (RR) transient measurements, for determining the interface recombination parameters of double-sided heterojunction solar cells. A physics-based model is developed, and normalized parameters are used to provide results that can be scaled to arbitrary wafer thickness and minority-carrier diffusion coefficient. In the case of dominant recombination at only one interface, interface recombination velocity can be extracted directly from RR times. In devices with significant recombination at both interfaces, numerical modeling must be used. The effects of minority-carrier current spreading in small devices can be corrected for analytically. The results are then applied to both PEDOT/n-Si and PEDOT/n-Si/TiO_2 heterojunction cells. We find that the PEDOT/n-Si interface, despite favorable band offsets and a significant built-in voltage, is not an ideal hole injector because of recombination at the PEDOT/n-Si interface. We also find that the effective surface recombination velocity at the Si-TiO_2 interface in a metallized device is 330 cm/s, confirming that the interface has a low defect density. Finally, we reflect on the significance of these results for the further development of silicon heterojunction cells.**

***Index Terms*— Device modeling, organic silicon, oxide silicon, reverse recovery (RR), silicon heterojunctions.**

I. Introduction

MONOCRYSTALLINE silicon solar cells, with their high material quality and well-understood physics, can boast of impressive efficiencies (~25% for lab cells) and significant commercial success, representing about 25% of all cell production in 2015 [1]. Recently, there has been growing interest in silicon heterojunction cells (SHJCs), which can offer the efficiencies of traditional silicon cells along with a decreased thermal budget and a potentially simpler manufacturing process. In these cells, the heavily doped side of a typical p^+-n or n^+-p-junction is replaced by an a-Si/Si [2], organic/Si [3]–[5], or metal oxide/Si heterojunction [6], [7] to create a carrier selective contact to lightly doped crystalline silicon. This contact blocks majority carriers from the lightly doped side from crossing to the contact in forward bias (thus greatly lowering dark current compared to a Schottky device), and the work function difference between the contact and the silicon creates an electric field that collects minority carriers generated by the sun.

Ideally, this contact serves as a minority-carrier injector into the silicon (n-type in our example). On the other side of the device, at the ohmic contact to the lightly doped semiconductor, a complementary heterojunction is used to block minority carriers in order to further reduce dark current. This effectively replaces the "backside field" implemented as an n/n^+ (or p/p^+) junction. Fig. 1(a) shows the dark current mechanisms in forward bias in such a device using PEDOT:PSS [poly(3,4-ethylenedioxythiophene) polystyrene sulfonate] and TiO_2 (titanium dioxide) as the electron and hole blockers, respectively, but the diagram would apply to other material configurations as well. The front (anode) contact supplies holes, which can recombine at the front electron-barrier/silicon interface ($J_{for,front}$) or be injected as minority carriers ($J_{for,inj}$) into the n-type bulk. Assuming no bulk recombination, they will then recombine at the rear hole-barrier/silicon interface. The rear cathode contact supplies electrons, which will either recombine at the rear interface or diffuse into the bulk and recombine at the front interface. This paper assumes that carriers do not penetrate their respective barriers.

A key issue in such cells is recombination at the two heterojunction interfaces to silicon, as indicated in Fig. 1(a). Recombination at either interface contributes to the dark current J_{for}. Because the dark current directly determines the open-circuit voltage, the interface recombination at both of these heterojunctions to silicon must be small to enable high cell performance. Inductively coupled photoconductivity decay measurements are widely used to measure effective minority-carrier lifetimes in high lifetime float-zone silicon

Manuscript received July 16, 2017; revised August 15, 2017 and August 17, 2017; accepted August 28, 2017. Date of publication September 18, 2017; date of current version October 20, 2017. This work was supported by the DOE Sunshot under Grant DE-EE0005315. The review of this paper was arranged by Editor A. G. Aberle. *(Corresponding author: Alexander H. Berg.)*

A. H. Berg and J. C. Sturm are with the Department of Electrical Engineering, Princeton Institute for the Science and Technology of Materials, Princeton University, Princeton, NJ 08544 USA (e-mail: ahberg@princeton.edu; sturm@princeton.edu).

K. A. Nagamatsu is with the Process Integration Group, Advanced Technology Laboratory of Northrop Grumman Corporation, Linthicum, MD 21090 USA (e-mail: ken.a.nagamatsu@gmail.com).

Color versions of one or more of the figures in this paper are available online at http://ieeexplore.ieee.org.

Digital Object Identifier 10.1109/TED.2017.2749525

0018-9383 © 2017 IEEE. Personal use is permitted, but republication/redistribution requires IEEE permission.
See http://www.ieee.org/publications_standards/publications/rights/index.html for more information.

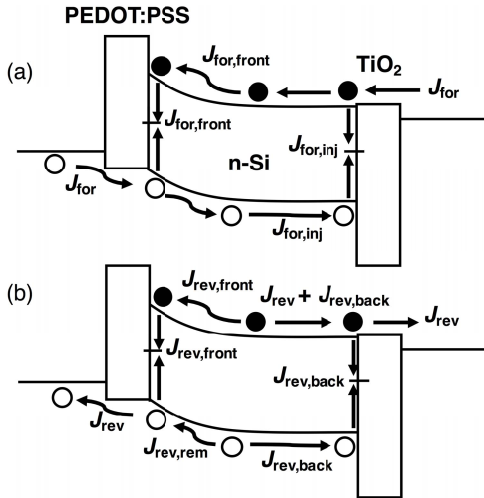

Fig. 1. (a) Band diagram of device in forward bias, with total current density J_{for}. Arrows show carrier flux direction. The PEDOT/Si serves as a minority-carrier injecting (major-carrier blocking) selective contact. Ignoring bulk recombination, injected holes can either diffuse through the bulk to the back ($J_{for,inj}$) or recombine at the front ($J_{for,front}$). The rear heterojunction (Si/TiO_2 in our case) serves as a selective contact that blocks minority carriers from recombining at the cathode contact in the ideal case, but in practice will allow a finite amount of interface recombination. (b) Bands and carrier flows during the reverse-current phase, again showing the front- and rear-interface recombination. Because the device voltage is approximately constant during this phase, the bands are essentially unchanged from the forward-current case.

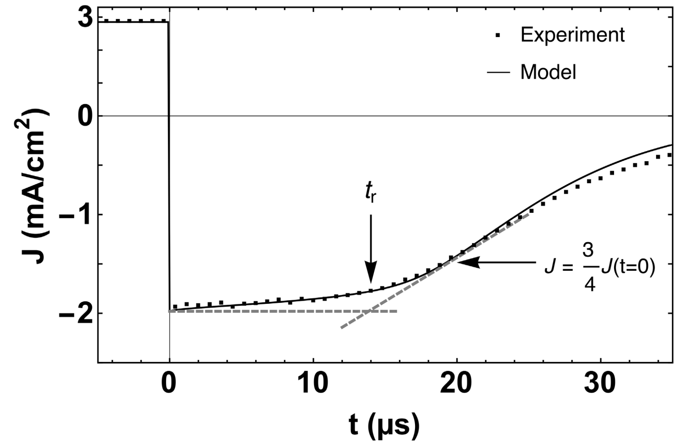

Fig. 2. Transient experimental and modeled results for a room-temperature PEDOT/n-Si device. Parameters are $J_{for} = 2.85$ mA/cm^2, $J_{rev,t=0} = 1.98$ mA/cm^2, $J_{for,front,t=0} = 0.63$ mA/cm^2, $\gamma_{area} = 0.88$, and $qV_{bi} = 0.7$ eV. Note the differing scales for positive and negative current density.

after heterojunction interfaces are deposited, allowing the extraction of minority-carrier recombination velocities at the interfaces [8]. However, subsequent contact metallization can cause chemical or electrical changes to the interface, greatly affecting recombination. The high conductivity of metal contacts means photoconductivity decay experiments cannot be carried out on metallized devices, so an alternative method is needed.

Previously, researchers have reported using modulated photoluminescence (MPL) [9], open-circuit voltage decay (OCVD) [10], and short-circuit current decay (SCCD) [11] to obtain recombination information. Compared to MPL, reverse recovery (RR) avoids problems that may arise due to the exciting illumination changing the effective recombination parameters, although we note that this effect may at times be useful. OCVD and SCCD are similar in concept to RR, and the basic ideas laid out here would also apply to those techniques; previous literature using these methods focuses only on back interface and bulk recombination, neglecting front-interface recombination, but could be extended along the lines presented here.

Using RR to extract the amount of recombination at both silicon interfaces in complete, contacted devices is the focus of this paper. Specifically, we will give a method that can be applied to the reverse bias transient current characteristics of SHJCs in general, and then use these results to measure this recombination in PEDOT/n-Si and PEDOT/n-Si/TiO_2 devices.

II. Reverse Recovery in Diodes With Minority Carriers

In an RR measurement, a constant forward current density J_{for} is applied across a minority-carrier diode for a time long enough to establish steady-state minority-carrier profiles in the silicon; this current is then quickly switched to a reverse current density J_{rev} by applying a reverse voltage to a resistor in series with the device under test (not directly to the device), and the transient current waveform is measured. For some time t_r, minority carriers stored in the device base can flow out through the front interface, and the current is approximately constant, defined by the voltage across the resistor. When these minority carriers begin to be significantly depleted, the current drops and eventually approaches the (negligible) device reverse-saturation current. As the current decreases, the diode voltage decreases; discharging of the device capacitance can affect the rate of the voltage decay as well. Typical data are shown in Fig. 2. Because the onset of the drop in voltage is not abrupt, for consistency we adopt the definition that t_r is the time when a line fit tangent to the J versus t curve at $J_{rev}(t) = 0.75 * J_{rev,t=0}$, where $J_{rev,t=0}$ is the reverse current immediately after the bias is switched from forward to reverse, intersects with the horizontal line through $J_{rev,t=0}$, as shown in Fig. 2.

Because hole transport in the n-type Si is governed by diffusion, J_{rev} has the effect of setting the slope of the hole concentration versus distance on the edge of the n-type region, adjacent to any space charge region. This slope remains constant during the length of the constant-current recovery phase. When the concentration of holes at this side reaches zero, at a time defined as $t = t_r$, that current (as reflected in the slope of minority-carrier density versus distance at the minority-carrier injecting interface) becomes untenable, and the current begins to decay, as can be seen in the final timepoints of Fig. 3.

This examination suggests that in low-level injection a 1-D diffusion equation model ought to be enough to model RR characteristics. The basic underlying equation is the time-dependent diffusion equation $\partial p/\partial t = D_p(\partial^2 p/\partial x^2)$, where p is hole density, q is the electron charge, and D_p is the hole diffusion constant. At the front interface, the external current $J_{ext} = -qD_p\partial p/\partial x + J_{front}$, where J_{ext} is the

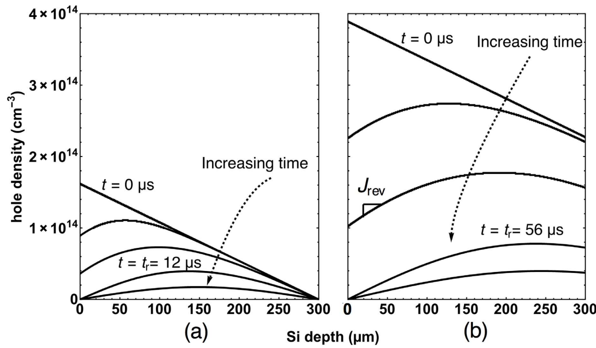

Fig. 3. Modeled hole profile across quasi-neutral region over time after reverse bias was applied for (a) PEDOT/n-Si device and (b) PEDOT/n-Si/TiO_2 device with the same forward-bias current density, assuming all current is carried by holes injected into the n-type base. The addition of the hole-blocking backside contact leads to a significantly increased number of holes in forward bias, and thus increased RR times. Parameters are $J_{for} = 10$ mA/cm^2, $J_{rev}(t = 0) = 15$ mA/cm^2, and $s_{Si/TiO_2} = 275$ cm/s, with $L = 0.03$ cm and base doping $n = 2 \cdot 10^{15}$ cm^{-3}.

externally measured current density and J_{front} is the front-interface recombination current density; this expression holds during both forward and reverse current periods. Note that J_{front} is defined to be always positive, so that during the forward current recombination adds to the externally measured current magnitude, whereas during the reverse current it subtracts from it. At the back interface, we have $-D_p \partial p/\partial x = p \cdot s_{back}$, again true during both forward and reverse periods. For a single-sided device (SSD), s_{back} is very high and the hole density at the back interface is effectively pinned at zero.

Kingston [12] examined the long-base diode to arrive at the expression $\mathrm{erf}[(t_r/\tau_p)^{1/2}] = (1 + J_{rev}/J_{for})^{-1}$, where τ_p is the bulk minority-carrier lifetime, while Grove and Sah [13] looked at the short-base-limiting case with infinitely fast recombination at the ohmic back contact. Neither of these conditions is applicable to a solar cell with a minority-carrier blocker— such a cell operates in the short-base regime (because of the high bulk lifetime) but should also have low recombination velocity at the back contact (because without low recombination the back heterojunction does not actually block minority flow). Furthermore, these models assume that the device current consists 100% of minority carriers injected in one direction at the junction—effectively an emitter efficiency of unity. Some recent studies of silicon heterojunction solar cells (see [14], [15]) have applied Kingston's equation to silicon heterojunction devices. Such fitting should be done cautiously, as experimental data may "fit" the long-base model even if the device itself is short-base or features nonidealities.

III. Reverse-Recovery Model With Interface Recombination

To extend previous work to a heterojunction device, one needs to account for recombination at the heterojunction interfaces. We restrict ourselves to interface recombination rather than depletion-region recombination because the latter should be small in high lifetime silicon. In the event that barrier tunneling is a significant effect, dark current resulting from it would be detected and measured by the following method, but it would not be separated out from "true" interface recombination current. Similarly, shunt currents (as long as they were small enough to not overwhelm the minority-carrier diffusion current) would also be detected as nonideal majority-carrier dark current. We separate our discussion into the effects of the two interfaces: that of the minority-carrier-hole blocking interface (the right side of Fig. 3) and the majority-carrier-electron blocking interface (the left side).

A. Recombination at Back Heterojunction Interface

We first consider the case where the only recombination is at the right interface in Fig. 1—the heterojunction that blocks injected minority-carrier holes from recombining at the cathode contact. We assume no recombination at the interface which blocks electrons from leaving the device, or equally the interface which injects minority carriers into the substrate.

We assume low-level injection current levels (no Auger recombination), and that equilibrium hole values are insignificant compared to the excited value, so that the hole current in the base is due only to diffusion and thus the local concentration gradient. Furthermore, assuming a hole barrier sufficiently thick to prevent direct tunneling and zero bulk recombination (high lifetime float-zone substrates were used in our experiments), the hole recombination rate at the back interface (and thus the transport rate across the substrate in steady state) is determined by the recombination rate at the back interface, $J_{for,inj} = q \cdot s_{back} \cdot p'_{back}$, where s_{back} is the surface recombination velocity at the back selective heterojunction and p'_{back} is the hole density at that interface. We assume a neutral back contact (flat silicon bands); band-bending up or down would increase or decrease the apparent recombination velocity, respectively.

Under forward bias, for the same voltage this contact reduces hole current by decreasing the magnitude of the hole gradient across the substrate, which, in the photovoltaic context, leads to an improvement in V_{OC}. In the RR context, for the same forward current, the layer [in a "double-sided device," (DSD)] leads to increases in both applied voltage and total stored holes over the "single-sided" heterojunction device SSD, as shown in Fig. 3.

Assuming no bulk recombination, low-level injection, and no recombination at the hole-injecting interface, it is straightforward to show that (at constant current) the presence of the minority-carrier blocker increases the number of initially stored holes according to

$$Q_{DSD} = Q_{SSD}\left(1 + \frac{2D_p}{L s_{back}}\right). \qquad (1)$$

This can be a significant difference: for parameters $L = 0.03$ cm, $D_p = 11.6$ cm^2/s, and $s_{back} = 250$ cm/s, the calculated increase is over 4×. Experimentally, s_{Si/TiO_2} as low as 75 cm/s has been reported in CVD-TiO_2 test structures measured via quasi-steady-state photoconductivity methods[16], which would lead to a change in t_r according to the model used here, of about 4× (the fact that this change matches the change in stored charge is coincidental and does not hold true generally).

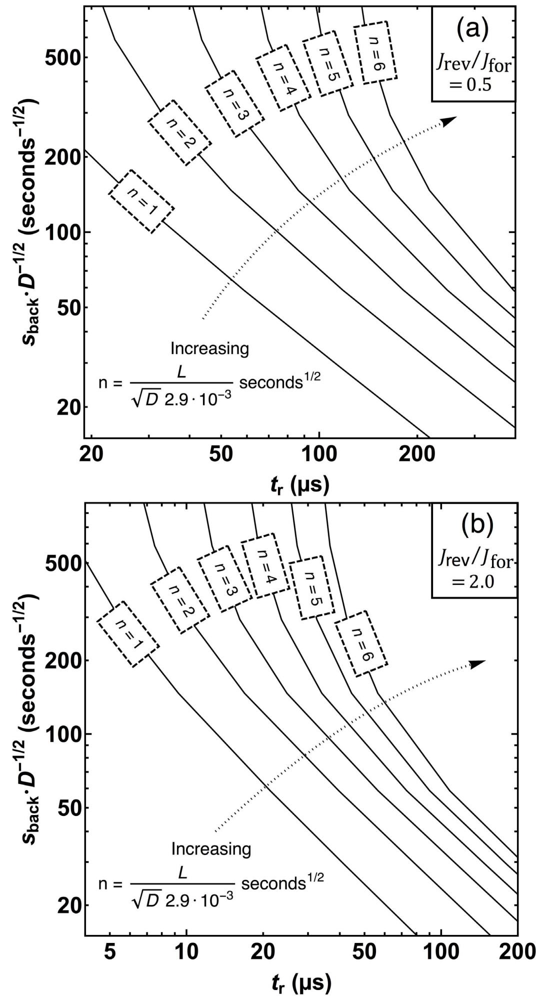

Fig. 4. Backside recombination velocity s_{back} as a function of RR time t_r in a DSD with ideal front interface, with (a) $J_{rev}/J_{for} = 0.5$ and (b) $J_{rev}/J_{for} = 2$ for a variety of $L/\sqrt{D}$ ratios.

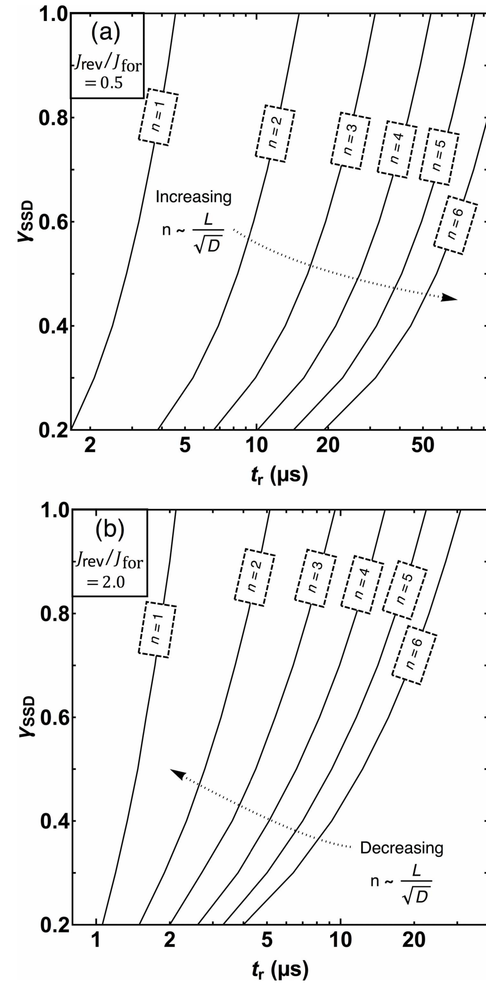

Fig. 5. Injection efficiency γ_{SSD} as a function of RR time t_r in a SSD, with (a) $J_{rev}/J_{for} = 0.5$ and (b) $J_{rev}/J_{for} = 2$, with $n = L/(\sqrt{D}{\cdot}2.9{\cdot}10^{-3})$.

Additionally, during the RR period itself, recombination at the back interface will consume holes faster at interfaces with higher recombination velocity. Because of the confluence of these two factors, a high quality back interface can increase recovery times by an order of magnitude for sufficiently low s_{back}.

Because the recovery time does not, in general, scale in proportion to the amount of stored charge, we instead used the diffusion equation and appropriate boundary conditions to model RR in devices with a perfect front interface ($s_{front} = 0$) for a variety of base thicknesses and s_{back} and J_{rev}/J_{for} values, with results presented in Fig. 4. (To enable side-by-side transient comparisons of the model results to real-world data, the model also included the circuit series resistance and coupling to the capacitive current source of the depletion region via the device voltage). For universal applicability, we use normalized units by dividing both s_{back} and the base thickness L by the square root of D, the minority-carrier diffusion constant, as well as by using J_{rev}/J_{for}. See the Appendix for details on these normalized variables. Figs. 4 and 5 also use $n = L/(\sqrt{D}\cdot 2.9 \cdot 10^{-3})$ to label curves; modeling parameters were chosen such that n takes integer values, as shown. Higher values of n require higher values of s_{back} to have the same resulting t_r, since devices using thicker wafers (or devices with smaller diffusion constants) store comparatively more charge for the same forward current.

Given the recovery time t_r, these curves allow the extraction of s_{back} in any device with an ideal minority-carrier injector and a back-interface heterojunction. For example, if one was testing a novel selective back contact to replace the back-surface field of a 0.02−cm-thick n-Si heterojunction with intrinsic thin layer cell, one might measure $t_r = 118$ μs at $J_{rev}/J_{for} = 0.5$; in this case, $n = 2$, and a consultation of Fig. 4 shows that this result corresponds to $s_{back}/\sqrt{D_p} \approx 59$ s$^{-1/2}$, or $s_{back} \approx 200$ cm/s. Because thinner devices store fewer carriers, a 0.01-cm-thick device with the same recovery time would have $s_{back} \approx 100$ cm/s.

B. Front Heterojunction Recombination in a Single-Sided Device

We now consider the effect of recombination at the minority-carrier-injecting heterojunction (left interface in Fig. 3). Recombination current at this interface affects the RR experiments in two distinct ways. First, during the forward-bias phase, any component of the current that does not lead to holes injected into the base does not create a stored charge to later be recovered. Therefore, in setting up the hole

distribution in the substrate in forward bias, the hole current density injected across the base is

$$J_{\mathrm{for,inj}} = \gamma_{\mathrm{SSD}} \cdot J_{\mathrm{for}} \tag{2}$$

with the emitter injection efficiency $\gamma_{\mathrm{SSD}} \equiv J_{\mathrm{for,inj}}/(J_{\mathrm{for,front}} + J_{\mathrm{for,inj}})$, so that the $J_{\mathrm{for,front}}$ reduces stored holes and thus the recovery time. We can incorporate this change into modeling by simply reducing the $J_{\mathrm{for,inj}}$ as in (2).

Second, during the RR phase, recombination ($J_{\mathrm{rev,front}}$) adds to the external current density J_{rev} flowing through the device terminals to give the total rate at which holes are being removed from the bulk, further reducing the recovery time compared to the case without such interface recombination. The hole-removal current density from the bulk at the front interface during the reverse transient is

$$J_{\mathrm{rev,rem}} = J_{\mathrm{rev}} + J_{\mathrm{rev,front}}. \tag{3}$$

Using the common PEDOT example, with the PEDOT highest occupied molecular orbital and the silicon valence band maximum closely aligned [17], the high doping of the PEDOT will pin the silicon Fermi level, leading to an interfacial hole density p_{int} that is high and, to first order, independent of voltage [18]. Given this, one can include the transient front-interface recombination in modeling via the expression

$$J_{\mathrm{rev,front}}(t) = J_{\mathrm{for,front}} \cdot \frac{p(0,t)}{p(0,0)} \tag{4}$$

even without knowing the values of the parameters (like interfacial defect density and capture cross section) that physically determine the recombination rate (note that, because tunneling or shunt currents do not follow this relationship, the presence of those would lead to a slightly worse fit between the model and experiment. However, because this is very much a second-order effect, we would not expect the change to be substantial). Equation (4) also suggests the definition $s_{\mathrm{front,eff}} = s_{\mathrm{front}} N_D/p_{\mathrm{int}}$, an effective recombination velocity for minority-carrier holes that accounts for the effects of a space charge region in the silicon at the interface. Given γ_{SSD}, a consideration of the hole profile across the base yields the expression

$$s_{\mathrm{front,eff}} = (D_p(1-\gamma_{\mathrm{SSD}}))/(\gamma_{\mathrm{SSD}} L). \tag{5}$$

Fig. 5 shows modeled (as in Section III-A) recovery times and their corresponding γ_{SSD} in short-base devices with an ohmic back contact. To test, for example, the properties of a novel oxide/silicon heterojunction injector with an inverted interface, one could use this information to analyze RR measurements and obtain both injection efficiency and the effective recombination velocity of the metallized junction. Recently, researchers showed how trap-saturation qualitatively affects the dynamics of PEDOT/n-Si junctions during the RR; [14] this method would allow the quantitative interpretation of their results.

C. Double-Sided Device With Two Nonideal Interfaces

The most complex device situation is a DSD with nonideal interfaces on both sides. The value of γ_{DSD} has significant effects on the extracted value of s_{back}. The two stored-charge loss mechanisms operate in parallel, and a single set of data may be explained by many pairs of their respective magnitudes. An analysis that omits front-interface recombination (i.e., assumes $\gamma_{\mathrm{DSD}} = 1$) will be able to be "fit" to experimental RR data, but the extracted s_{back} might be many times larger than the true value obtained by incorporating an accurate $\gamma_{\mathrm{DSD}} \neq 1$.

To determine the parameters of such devices, the following method may be used.

1) Measure RR in an SSD (e.g., PEDOT/n-Si) with an ohmic back contact.
2) Fit to 1-D short-base diffusion modeling (Fig. 5) to find γ_{SSD} and thus $s_{\mathrm{front,eff}}$, as described in Section III-B and using (5).
3) Measure RR in a DSD (e.g., PEDOT/n-Si/TiO_2) and fit to numerical solutions of the diffusion equation with recombination at both sides, subject to the condition

$$\gamma_{\mathrm{DSD}} = \left[1 + \frac{s_{\mathrm{front,eff}}}{s_{\mathrm{back}}}\left(1 + \frac{L s_{\mathrm{back}}}{D_p}\right)\right]^{-1} \tag{6}$$

which can be derived by considering the relationship between base hole profile, steady-state current, and the definition of s. This is a coupled fitting; each s_{back} fitting attempt necessitates a new value for $J_{\mathrm{for,front}}$. As an example, this method is applied to experimental data in Section V.

IV. Current-Spreading Effects

In devices with long bulk lifetimes, carriers will diffuse laterally away from the device. If this distance is significant compared to the device dimensions, the behavior of the 3-D hole distribution will not be identical to that predicted by 1-D models for the same amount of total current. One could compensate for this effect by using an effective 1-D forward current density

$$J_{\mathrm{for,1-D,eff}} = J_{\mathrm{for,experiment}} \cdot \gamma_{\mathrm{area}} \tag{7}$$

where γ_{area} is the some size-dependent factor whose value is not immediately obvious.

To investigate this phenomenon, we carried out full 3-D numerical RR simulations of p^+n-diodes (with no back-side field) in a commercial modeling tool for a number of different device radii (Fig. 6). From the point of view of minority carriers in the substrate, p^+n devices are similar to short-base heterojunction devices with near-perfect carrier injection efficiency, making them applicable for a study specifically of current spreading. The simulation parameters were $J_{\mathrm{for}} = 10.1$ mA/cm^2, $p^+ = 10^{20}$ cm^{-3}, $n = 2 \cdot 10^{15}$ cm^{-3}, and $L = 0.03$ cm. To further isolate the effect of current spreading, we assumed zero bulk recombination, zero top-surface recombination outside the device area, and an ohmic back contact on the entire backside.

Smaller devices had uniformly shorter recovery times for the same current densities; in those devices, the current is significantly spread out from the contacted device area, and spread-out carriers are less likely to be recovered during the reverse transient.

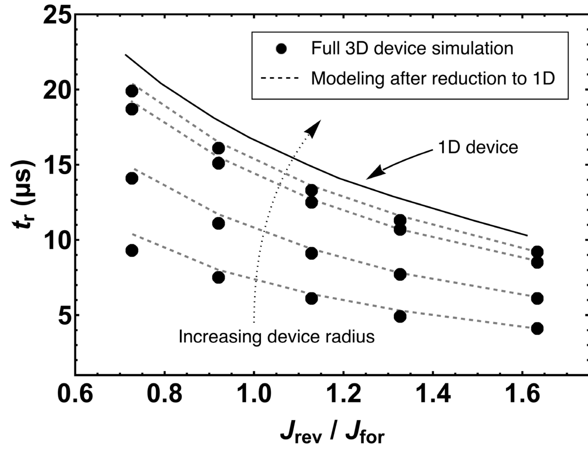

Fig. 6. RR times for short-base p^+n-diodes as a function of J_{rev}/J_{for} by full 3-D device simulation and by modeling after reduction to 1-D. Also shown is the modeled time for a fully 1-D device, which is the limiting case of increasing device radius. Devices are circular with radii (top to bottom) of 2.5, 1.5, 0.5, and 0.25 mm. $J_{for} = 10.1$ mA/cm^2. The size-dependent reduction allows us to analyze the 3-D RR problem using its 1-D equivalent.

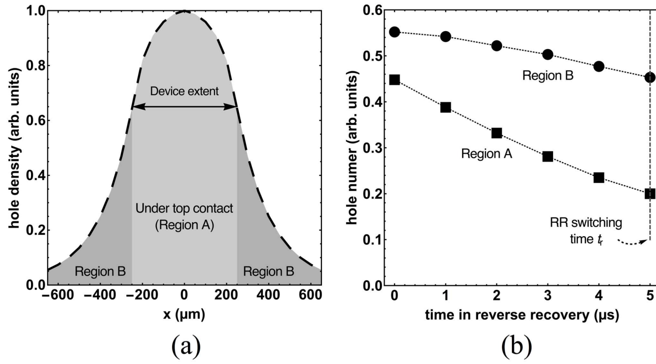

Fig. 7. (a) Hole density (cm^{-2}, arbitrary units) in forward bias, obtained by integrating hole density from the top to the bottom of the wafer for a single slice along the device diameter, of a simulated 250-μm-radius 3-D p^+n-diode, showing region A (under the contacted device area) and region B (the rest of the substrate). (b) 3-D-integrated hole number (each normalized to total hole number), in each of the two regions, over time in an RR simulation of this device with $J_{for} = 10.1$ mA/cm^2 and $J_{rev} = 13.4$ mA/cm^2. Despite the fact that initially region B contains 55% of all stored holes, significantly more holes are extracted from region A than from region B during the RR process.

To quantify this effect, we examined the hole distribution in the substrate during the reverse transient by 3-D device simulation. Fig. 7(a) shows the hole density (in number per cm^2, arbitrary units), obtained by integrating hole density from the top to the bottom of the wafer for a single slice along the device diameter. The total number of stored holes could be broken up into two parts: those directly under the device (region A) and those that had "spread out" (region B); totals in each region were obtained by integrating in all three dimensions. During the recovery transient [Fig. 7(b)], the number of holes in region B decreases only slightly before the RR time t_r, when the reverse current begins to drop; the recovered holes that supply the reverse transient current come almost entirely from region A. Proportionally, the difference is even greater. Thus, the relevant forward current for purposes of RR is that directly under the contact area—those are the carriers that are later collected. In other words, γ_{area} = current in region A/total current.

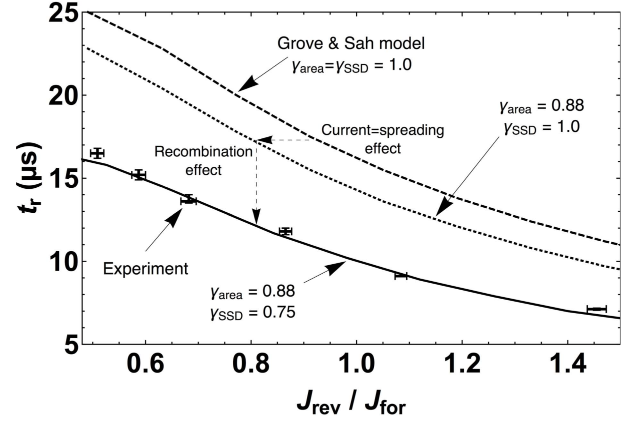

Fig. 8. Data and model fits for a PEDOT/n-Si device, with $J_{for} = 2.85$ mA/cm^2 for all data points. The best fit line accounts for both current spreading ($\gamma_{area} = 0.88$, found by the method in [19]) and front-interface recombination ($\gamma_{SSD} = 0.75$).

This ratio was fortunately derived in [19], which gives a system of equations that can be solved numerically for the desired result γ_{area} (denoted there as I_{1-D}/I_{2-D}). To test this method, we used this γ_{area} to adjust the 3-D-simulated total forward current density J_{for} according to (7) (J_{rev} remains unchanged, since nearly all reverse current is coming from the region under the contact), and then modeled in 1-D as described in Section III-B. The resulting 1-D-modeling curves (Fig. 6) line up closely with the fully simulated 3-D curves; agreement is nearly exact for $J_{rev} \geq J_{for}$, with small deviations for low J_{rev}/J_{for} (within 10%), showing that this simple procedure can be used to effectively reduce the experimental results to their 1-D equivalents, which can be more easily analyzed. In summary, then, when devices are small, the modeling described in Section III must also include this area-modification factor γ_{area}.

V. Application to Experimental Results

Both SSD and DSD were fabricated using lightly doped ($N_D \approx 2 \cdot 10^{15}$ cm^{-3}) 0.03-cm-thick float-zone substrates. On the front, 70 nm of PEDOT:PSS was spun on to serve as a hole-selective injector; to make DSDs, 3-nm TiO_2 was additionally deposited on the back via CVD to make a hole-blocking contact, with Al contacts deposited via thermal evaporation. The device size was 0.4 cm × 0.4 cm. Further details are given in [20]. RR measurements were carried out over a range of reverse biases for each of several forward biases. The voltage switching times and parasitic capacitances were relevant only on time scales less than 1 μs, much less than the recovery times of our devices, which were typically 10–100 μs. Based on [4] and [18], we set the model's built-in voltage to $V_{bi} = 0.7$ V.

We first present results for SSDs. Fig. 8 shows the experimental results for t_r as a function of J_{rev}/J_{for} for a PEDOT/n-Si device with $J_{for} = 6.35$mA/cm^2. The Grove and Sah prediction of t_r, which has no adjustable parameters and implicitly assumes $\gamma_{SSD} = \gamma_{area} = 1$, is also plotted. The results of the Grove and Sah model, which significantly overestimates t_r for all J_{rev}/J_{for}, were then corrected for current spreading (which causes many injected carriers to not

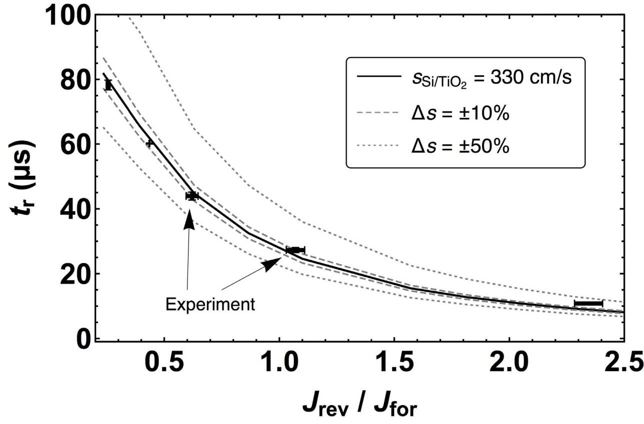

Fig. 9. Data and model fits for a PEDOT/n-Si/TiO_2 device, with J_{for} = 6.35 mA/cm^2, γ_{area} = 0.79, and $J_{for,front,t=0}$ = 2.11 mA/cm^2. Dashed and dotted lines show the effect of changing s_{Si/TiO_2} by 10% and 50%, respectively.

be recovered) using the approach of Section IV. Including the resulting factor (γ_{area} = 0.88) to account for current-spreading, essentially shifting the t_r versus J_{rev}/J_{for} left, is not enough to account for all of the overestimation.

The Grove and Sah model also implicitly assumes that all forward current injects minority carriers which are later collected—in other words, that $\gamma_{SSD} = 1$. We adjusted γ_{SSD} to achieve a best fit of the model to experiment, as in Section III-B, with $\gamma_{SSD} = 0.75$ giving excellent agreement. This means that 25% of the forward-bias current is due to nonideal recombination at the PEDOT/n-Si interface. This fact has important ramifications for the improvement of V_{OC} via a lowering of the dark current. A strategy that aims only at selectively passivating the backside contact will be able to reduce the hole diffusion current but will not affect the front-interface recombination current, limiting the possible V_{OC} improvement.

Based on this result, we used (5) to find $s_{PEDOT/Si,eff}$ = 130 cm/s. This low value is, we emphasize, not due solely to chemical passivation at the interface, but rather to chemical passivation combined with the significant band-bending imposed by the high PEDOT:PSS work function.

We next measured the RR in double-sided PEDOT/n-Si/TiO_2 devices and modeled the data using the results of single-sided measurements ($s_{PEDOT/Si,eff}$ = 130 cm/s) to include the effects of emitter inefficiency as in Section III-C (Fig. 9). J_{for} was also adjusted to account for the effects of current spreading as in Section IV. There was a single fitting parameter, s_{Si/TiO_2}, which was found to have a value of s_{Si/TiO_2} = 330 cm/s, a number in line with previous measurements of that interface [20]. This demonstrates that the interface remains relatively stable, even after contact deposition. Additional curves in Fig. 9 show the effects on the model of changing s_{Si/TiO_2} by ±10% and 50%, indicating sensitivity to the fitting parameter. These results suggest that the transient RR method can fix the backside recombination velocity of complete, contacted devices to within approximately 10%.

We also note that because of the reduced minority-carrier current in the DSD versus SSD for a given forward bias, the minority-carrier injection ratio is decreased in the DSD versus SSD, from $\gamma_{SSD} = 0.75$ to $\gamma_{DSD} = 0.58$; in other words, nearly half of the forward-bias current in this device is due to front-interface recombination.

VI. Conclusion

We have developed a flexible RR method to identify the effects of interface recombination at both silicon surfaces in silicon heterojunction solar cells. The analyses shown here allow the direct extraction of the recombination characteristics of novel heterojunction emitters and selective contacts; we also detail a method for parameter extraction in cases where both front and back interfaces are nonideal. The analysis is further extended to include the effects of current spreading in small-area devices. We applied this method to investigate the current mechanisms in PEDOT/n-Si(/TiO_2) devices. The PEDOT/n-Si junction under study was found to be a significantly nonideal minority-carrier injector, with injection efficiencies as low as 75% in devices without a TiO_2 hole-blocking cathode at room temperature. The effective interface recombination velocity at the TiO_2 interface was found to be 330 cm/s, similar to that achieved by back-surface fields created via rapid thermal processing of screen-printed Al layers [21].

These results suggest that the PEDOT/Si junction, while of remarkably high quality for being an organic/inorganic and amorphous/crystalline interface, may become a limiting factor as devices built around it are optimized. If recombination at that interface remains significant, it will be imperative for researchers to develop alternative hole-injecting interfaces that more closely approach the quality of high-temperature diffused junctions.

Appendix

The RR process depends on the wafer thickness and minority-carrier diffusion constant D. To make our numerical modeling results more general, we define normalized variables for distance and interface recombination velocity. In the device bulk (for n-Si), the time-dependent minority-carrier diffusion equation is

$$\frac{\partial p}{\partial t} = D_p \frac{\partial^2 p}{\partial x^2} \tag{8}$$

$$= D_p \frac{\partial}{\sqrt{D_p}\partial(x/\sqrt{D_p})} \frac{\partial}{\sqrt{D_p}\partial\ (x/\sqrt{D_p})} p \tag{9}$$

$$= \frac{\partial^2 p}{\partial (x')^2} \tag{10}$$

which is independent of D_p. Thus, we define a normalized length scale $x' \equiv x/\sqrt{D_p}$, implying a normalized wafer thickness $L' \equiv L/\sqrt{D_p}$. At the back interface, where the hole current toward the contact equals the recombination rate at the interface

$$D_p \frac{\partial p}{\partial x} = -s_{back}\, p \tag{11}$$

$$\sqrt{D_p} \frac{\partial p}{\partial x'} = -s'_{back} \sqrt{D_p} \cdot p \tag{12}$$

$$\frac{\partial p}{\partial x'} = -s'_{back}\, p. \tag{13}$$

Thus, we define a normalized $s'_{back} \equiv s_{back}/\sqrt{D_p}$.

Finally, at the front interface

$$J = -qD_p\frac{\partial p}{\partial x} + J_{\text{front}} \tag{14}$$

$$J = -q\sqrt{D_p}\frac{\partial p}{\partial x'} + J_{\text{front}} \tag{15}$$

$$J' = -q\frac{\partial p}{\partial x'} + J'_{\text{front}} \tag{16}$$

where we defined normalized current densities $J_i' = J_i/\sqrt{D_p}$ for both currents in equation. The numerical modeling is then done in terms of these normalized variables and ratios of normalized currents, as presented in Figs. 4 and 5. Given the wafer thickness and appropriate diffusion constant, the results of Figs. 4 and 5 can be scaled to the specific experiment of interest.

References

[1] Fraunhofer Institute. Annual Energy Outlook. (2016). *Photovoltaics Report*. [Online]. Available: https://www.ise.fraunhofer.de/content/dam/ise/de/documents/publications/studies/Photovoltaics-Report.pdf

[2] S. de Wolf, A. Descoeudres, Z. C. Holman, and C. Ballif, "High-efficiency silicon heterojunction solar cells: A review," *Green*, vol. 2, pp. 7–24, Jan. 2012, doi: 10.1515/green-2011-0039.

[3] S. Avasthi, S. Lee, Y. L. Loo, and J. C. Sturm, "Role of majority and minority carrier barriers silicon/organic hybrid heterojunction solar cells," *Adv. Mater.*, vol. 23, no. 48, pp. 5762–5766, 2011, doi: 10.1002/adma.201102712.

[4] A. S. Erickson, A. Zohar, and D. Cahen, "n-Si–organic inversion layer interfaces: A low temperature deposition method for forming a p–n Homojunction in n-Si," *Adv. Energy Mater.*, vol. 4, no. 9, pp. 1–4, 2014, doi: 10.1002/aenm.201301724.

[5] K. A. Nagamatsu, S. Avasthi, J. Jhaveri, and J. C. Sturm, "A 12% efficient silicon/PEDOT:PSS heterojunction solar cell fabricated at <100 °C," *IEEE J. Photovolt.*, vol. 4, no. 1, pp. 260–264, Jan. 2014, doi: 10.1109/JPHOTOV.2013.2287758.

[6] C. Battaglia *et al.*, "Silicon heterojunction solar cell with passivated hole selective MoO_x contact," *Appl. Phys. Lett.*, vol. 104, no. 11, p. 113902, 2014, doi: 10.1063/1.4868880.

[7] L. G. Gerling *et al.*, "Transition metal oxides as hole-selective contacts in silicon heterojunctions solar cells," *Solar Energy Mater. Solar Cells*, vol. 3, pp. 1–7, Feb. 2015, doi: 10.1016/j.solmat.2015.08.028.

[8] R. A. Sinton, A. Cuevas, and M. Stuckings, "Quasi-steady-state photoconductance, a new method for solar cell material and device characterization," in *Proc. 25th IEEE Photovolt. Specialists Conf. Rec.*, May 1996, pp. 457–460.

[9] R. Brüggemann and S. Reynolds, "Modulated photoluminescence studies for lifetime determination in amorphous-silicon passivated crystalline-silicon wafers," *J. Non-Cryst. Solids*, vol. 352, nos. 9–20, pp. 1888–1891, 2006, doi: 10.1016/j.jnoncrysol.2005.11.092.

[10] F. A. Lindholm, J. J. Liou, A. Neugroschel, and T. W. Jung, "Determination of lifetime and surface recombination velocity of p-n junction solar cells and diodes by observing transients," *IEEE Trans. Electron Devices*, vol. ED-34, no. 2, pp. 277–285, Feb. 1987, doi: 10.1109/T-ED.1987.22919.

[11] T.-W. Jung, F. A. Lindholm, and A. Neugroschel, "Unifying view of transient responses for determining lifetime and surface recombination velocity in silicon diodes and back-surface-field solar cells, with application to experimental short-circuit-current decay," *IEEE Trans. Electron Devices*, vol. ED-31, no. 5, pp. 588–595, May 1984, doi: 10.1109/T-ED.1984.21573.

[12] R. H. Kingston, "Switching time in junction diodes and junction transistors," *Proc. IRE*, vol. 28, no. 5, pp. 829–834, May 1954, doi: 10.1109/JRPROC.1954.274521.

[13] A. S. Grove and C. T. Sah, "Simple analytical approximations to the switching times in narrow base diodes," *Solid State Electron.*, vol. 7, no. 1, pp. 107–110, 1964, doi: 10.1016/0038-1101(64)90128-5.

[14] A. B. Prakoso, L. Ke, J. Wang, Z. Li, C. Jiang, and Rusli, "Reverse recovery transient characteristic of PEDOT:PSS/n-Si hybrid organic-inorganic heterojunction," *Org. Electron.*, vol. 42, pp. 269–274, Mar. 2017, doi: 10.1016/j.orgel.2016.12.022.

[15] Y. Jung, X. Li, N. K. Rajan, A. D. Taylor, and M. A. Reed, "Record high efficiency single-walled carbon nanotube/silicon p–n junction solar cells," *Nano Lett.*, vol. 13, no. 1, pp. 95–99, 2013, doi: 10.1021/nl3035652.

[16] J. Jhaveri *et al.*, "Double-heterojunction crystalline silicon solar cell with electron-selective TiO_2 cathode contact fabricated at 100 °C with open-circuit voltage of 640 mV," in *Proc. IEEE 42nd Photovolt. Specialists Conf. (PVSC)*, vol. 2. Jun. 2015, pp. 3–6, doi: 10.1109/PVSC.2015.7356054.

[17] G. Greczynski, T. Kugler, M. Keil, W. Osikowicz, M. Fahlman, and W. R. Salaneck, "Photoelectron spectroscopy of thin films of PEDOT–PSS conjugated polymer blend: A mini-review and some new results," *J. Electron Spectrosc. Rel. Phenomena*, vol. 121, nos. 1–3, pp. 1–17, 2001, doi: 10.1016/S0368-2048(01)00323-1.

[18] S. Jäckle *et al.*, "Junction formation and current transport mechanisms in hybrid n-Si/PEDOT:PSS solar cells," *Sci. Rep.*, vol. 5, p. 13008, Aug. 2015, doi: 10.1038/srep13008.

[19] P. J. Chen, K. M. Misiakos, A. Neugroschel, and F. A. Lindholm, "Analytical solution for two-dimensional current injection from shallow p-n junctions," *IEEE Trans. Electron Devices*, vol. ED-32, no. 11, pp. 2292–2296, Nov. 1985, doi: 10.1109/T-ED.1985.22272.

[20] K. A. Nagamatsu *et al.*, "Titanium dioxide/silicon hole-blocking selective contact to enable double-heterojunction crystalline silicon-based solar cell," *Appl. Phys. Lett.*, vol. 106, no. 12, p. 123906, 2015, doi: 10.1063/1.4916540.

[21] S. Peters, "Rapid thermal processing of crystalline silicon materials and solar cells," Ph.D. dissertation, Dept. Phys., Univ. Konstanz, Konstanz, Germany, 2004.

Alexander H. Berg (S'15) received the B.S. degree in engineering-physics from Brown University, Providence, RI, USA, in 2013, and the M.A. degree in electrical engineering from Princeton University, Princeton, NJ, USA, in 2015, where he is currently pursuing the Ph.D. degree in electrical engineering.

His current research interests include the modeling and material science of hybrid silicon heterojunctions for photovoltaic applications.

Ken A. Nagamatsu received the B.S. degree in microelectronic engineering from the Rochester Institute of Technology, Rochester, NY, USA, in 2010, and the M.A. and Ph.D. degrees in electrical engineering in 2012 and 2016, respectively.

He is currently a Process Integration Engineer with the Advanced Technologies Laboratories, Northrop Grumman Mission Systems, Linthicum, MD, USA. His current research interests include superlattice devices in gallium nitride for high-frequency RF applications.

James C. Sturm (S'81–M'85–SM'95–F'01) received the B.S.E. degree in electrical engineering and engineering physics from Princeton University, Princeton, NJ, USA, in 1979, and the M.S.E.E. and Ph.D. degrees from Stanford University, Stanford, CA, USA, in 1981 and 1985, respectively.

In 1986, he joined the Faculty of Princeton University, where he is currently the Stephen R. Forrest Professor in electrical engineering.